

IIT Hyderabad

Kirigami Soft Gripper

Submitted by:

ME21BTECH11001 Abhishek Ghosh

ME21BTECH11002 Aditya Verma

ME21BTECH11043 Raman Kumar

ME5053: Soft Robotics

Mechanical Engineering

03.03.2024

Submitted to:

Dr. Prakhar Gupta

Contents

1	Introduction	2
2	Kirigami Shell Design and Pattern Selection	2
3	Variation of Appendages	3
4	Evaluation on Frictions	4
5	Theoretical Modeling	4
5.1	Skew Shell	4
5.2	Elastic Hinge	8
6	Conclusion	10

1 Introduction

Soft robotics is a rapidly growing field that aims to develop flexible and adaptable robotic systems. One of the innovative designs in this domain is the kirigami soft gripper, which uses patterned cuts and shape-morphing mechanisms to achieve grasping and manipulation. This report explores the design principles, simulations, experimental evaluations, and theoretical modeling of the kirigami gripper, based on the supplementary materials of the research paper.

2 Kirigami Shell Design and Pattern Selection

Kirigami, derived from the Japanese art of paper cutting, enables structures to undergo large deformations without requiring additional actuators. The key design parameters of a kirigami shell include:

- Slit length l_c
- Slit width t_c
- Longitudinal spacing l_y
- Transverse spacing l_x

For effective grasping, the pattern must satisfy:

$$l_y/l_x > 1 \quad (1)$$

$$l_y/\sqrt{(\frac{l_c}{2} - \frac{l_x}{2})^2 + (l_y - t_c)^2} > 0.75 \quad (2)$$

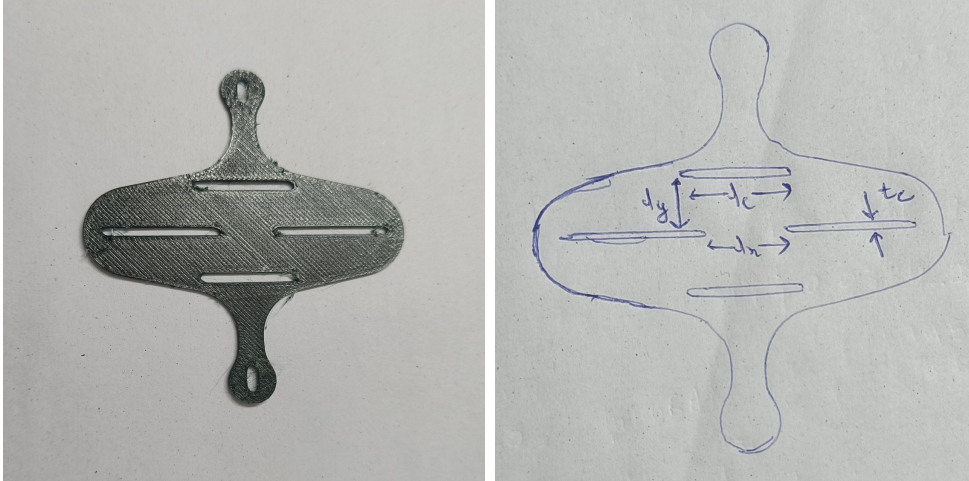


Figure 1: Kirigami Soft Gripper

By satisfying these constraints, the shell can trap elastic energy and form periodic ridges or valleys, leading to effective shape-morphing for gripping. In contrast, when a principal curvature of finite and arbitrary magnitude is introduced along the transverse direction (perpendicular to the loading direction), the kirigami-patterned shell deforms

into a cylindrical metasurface upon stretching (Fig. 1). This transformation is independent of the size or overall geometry of the kirigami shell and is instead dictated by the aforementioned geometric parameters.

Some key observations:

- Kirigami shells wrap into cylindrical metasurfaces when stretched.
- Stress concentration occurs at the slit tips, leading to localized plastic deformation.
- The appendage shape (rectangular, circular, flipper-like) affects object handling but not gripping capacity.

3 Variation of Appendages

Shape morphing occurs due to the deformation of skew shells and hinges, while the appendages remain underactuated. All kirigami patterns share the same geometric parameters.

At full closure, when the appendages touch, the gap between contact points forms an opening that determines the smallest object the gripper can hold. While the appendage shape does not affect the overall holding capacity, it influences the size and shape of objects that can be gripped.

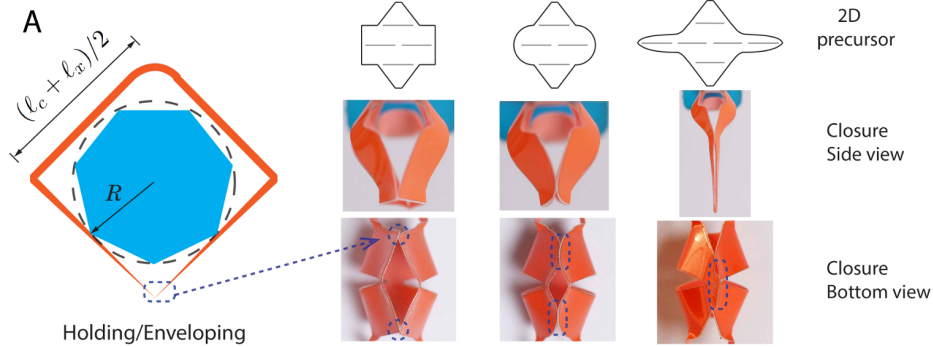


Figure 2: Appendages Analysis

Whether an object can be fully enclosed depends on its size and shape relative to the kirigami shell geometry. As shown in Fig. 2, for complete enclosure, a simple geometric constraint must be met:

$$\pi R < l_c + l_x \quad (3)$$

where R is the radius of the sphere. If the object is a regular shape, such as a polygon, R represents the radius of its circumcircle. This constraint defines the upper size limit for full enclosure.

The smallest grippable object size is determined by the contact points of the appendages at full closure. As the appendage shape transitions from rectangular to half-circle to flipper-like in the 2D precursor, the diamond-shaped opening decreases (Fig. S2). If the object is smaller than this opening, it may not be securely held, setting a lower size limit for grasping.

4 Evaluation on Frictions

The friction force acting on the interfaces between the appendages and the object during the pulling-out process is considered as kinetic friction, denoted by f_k , as shown in Fig. 3. This kinetic friction is calculated as $f_k = \mu_k F_N$, where, μ_k is the kinetic friction coefficient. The force balance between F_p , F_N , and f_k gives, $F_p = 2(F_N \cos \alpha + f_k \sin \alpha)$. Substituting $f_k = \mu_k F_N$ into the above equation yields,

$$F_p = 2F_N(\cos \alpha + \mu_k \sin \alpha) \quad (4)$$

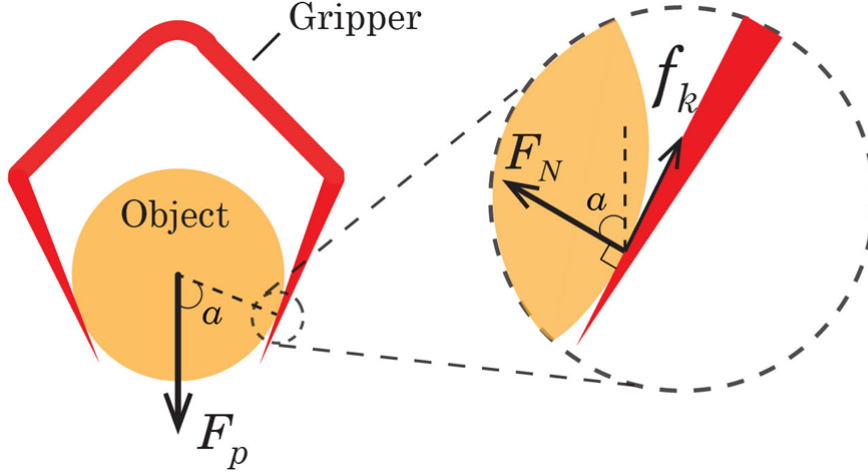


Figure 3: Friction Analysis

By ignoring the friction (let $k = 0$), we may underestimate the force required to pull out the object from the gripper. In other words, friction enhances the holding capacity of the gripper.

5 Theoretical Modeling

In this section, we present the detailed theoretical model for understanding the mechanical response and gripping optimization of the kirigami shell. Here, we only consider the shape shifting unit (skew shell and elastic hinge) of the kirigami shell.

5.1 Skew Shell

The deformation of the skew shell is very complicated and there is no closed-form analytical solution. To provide insight, we make assumptions and simplify the problem based on results from numerical simulations. As shown in Fig.4, we marked each vertex of the shell and observed the relative deflection between edge 1-4 and edge 2-3. Note that the displacement of the shell with respect to the undeformed configuration is a superposition of displacement induced by bending of the skew shell and rotation of the elastic hinge. Thus, relative deflection is used to evaluate bending of the skew shell. We converted the skew shell into a cylindrical shell with an equivalent length of $L_e = \sqrt{(\frac{l_c}{2} - \frac{l_x}{2})^2 + (l_y - t_c)^2}$ and width of $b = l_y - t_c$. By using the relative deflections, we compared the tip deformation of

edge 1-2 and edge 3-4 with the unskewed shell simplification. The result indicated that by only considering the vertical deflection (δ), the unskewed equivalent model may be used to predict the deflection of the skew shell components with underestimation. Here, the difference between edge 1-2 and edge 3-4 is caused by torsion induced by skew shell bending.

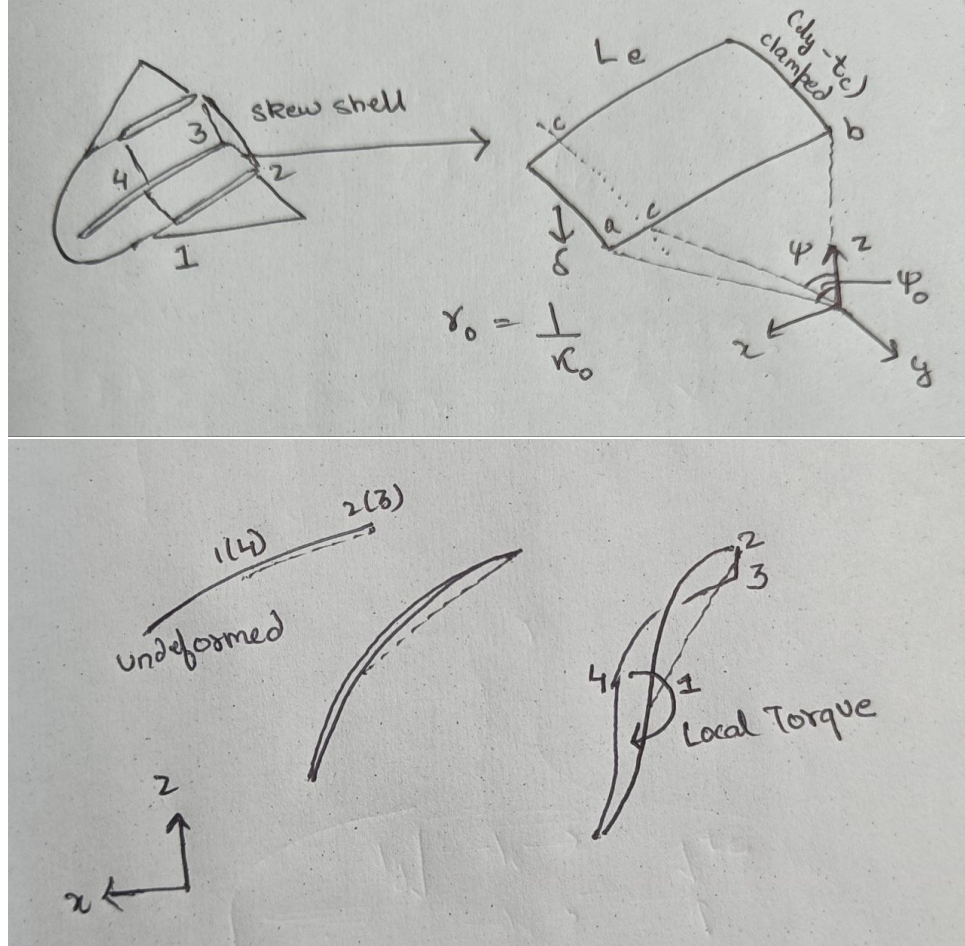


Figure 4: Skew Shell

Although the deformation of the skew shell is very complicated due to the combination of the loading conditions, we showed that the elastic energy is mainly dominated by bending energy in the main text.

Numerical Analysis:

In general, elastic energy of a thin shell can be expressed as:

$$U_s \approx U_s^b = \frac{D}{2} \iint (k_{xx} + k_{yy})^2 + 2(1-\nu)(k_{xy}^2 - k_{xx}k_{yy}) dx dy$$

where,

$K(x,y)$: curvature, $D = \frac{Eh^2}{12(1-\nu^2)}$ (Flexural rigidity according to Kirchhoff-Love thin shell theory)
 ν : Poisson's ratio

Assuming material is isotropic ($K_{xy} = K_{yx} = 0$)

Hence,

$$U_s^b = \frac{D}{2} \iint (k_{xx})^2 dx dy$$

using relation: $M_{xx} = D k_{xx}$

$$U_s^b = \frac{1}{2Db} \int (M_{xx})^2 dy \quad b = l_y - t_c \text{ (width of shell)}$$

To calculate the bending moment, we are using polar coordinate for convenience,

from image,

$$dx = R_0 d\varphi$$

bending moment at any moment cross section:

$$M_c(\varphi) = P(\delta) (R_0 \sin \varphi_0 - R_0 \sin \varphi)$$

$P(\delta)$ = force induced by displacement δ .

$$U_s^b = \frac{1}{2Db} \int_0^{\varphi_0} [M_c(\varphi)]^2 d\varphi$$

$$U_s^b = \frac{P(\delta)^2 R_0^3}{2D(l_y - t_c)} \int_0^{\varphi_0} (\sin \varphi_0 - \sin \varphi)^2 d\varphi$$

external work done = elastic energy yielding $\Rightarrow U_s^b$

$$U_s^b = \frac{1}{2} P(\delta) \delta$$

$$\Rightarrow 2 \frac{U_s^b}{\delta} = P(\delta)$$

$$U_s^b = \frac{D(l_y - t_c) \delta^2}{2R_0^3 \int_0^{\varphi_0} (\sin \varphi_0 - \sin \varphi)^2 d\varphi}$$

$$\text{since } R_0 = \frac{Le}{\varphi_0}$$

$$U_s^b = \frac{D(l_y - t_c) \varphi_0^3 \delta^2}{Le^3 [\varphi_0 + 2\varphi_0 \sin^2 \varphi_0 + \sin^2 \varphi_0 (3 \cos \varphi_0 - 4)]}$$

Figure 5: Skew Shell Numerical Analysis

Bending energy of elastic hinge

$$U_h^b = D(1+\nu)\beta(2\theta)$$

where β is sector angle as shown in fig.

Because principal curvature is very small, $\beta = d_2 \kappa_b$,
 κ_b is curvature at clamped end.

$$\kappa_b = \frac{M_b}{D(d_y - t_c)}$$

where,

$$M_b = P(\delta) \varphi_0 \sin \varphi_0 = \frac{D(d_y - t_c) \delta}{L_a^2} \frac{2 \varphi_0^2 \sin \varphi_0}{\varphi_0 + 2 \varphi_0 \sin^2 \varphi_0 + \sin \varphi_0 (3 \cos \varphi_0 - 4)}$$

$$\Rightarrow U_h^b = \frac{4(1+\nu) D d_2 \varphi_0^2 \sin \varphi_0}{L_a^2 [\varphi_0 + 2 \varphi_0 \sin^2 \varphi_0 + \sin \varphi_0 (3 \cos \varphi_0 - 4)]}$$

$$\text{where, } D = \frac{E h^3}{12(1-\nu^2)}$$

We define energy ratio,

$$\frac{U_s^b}{U_s^b + U_h^b} = \frac{1}{1 + \lambda_g \theta / d}$$

We define girder char. length λ_g as

$$\lambda_g = 4(1+\nu) \frac{d_2 \sin(\kappa_b L_c)}{(d_y - t_c) \kappa_b}$$

We non-dimensionalize this,

$$\frac{d_c}{\lambda_g} = \frac{d_c \kappa_b \left(\frac{d_y}{d_c} - \frac{t_c}{d_c} \right)}{4(1+\nu) \frac{d_2}{d_c} \sin \left(\kappa_b L_c \sqrt{\left(\frac{1}{2} - \frac{d_2}{2d_c} \right)^2 + \left(\frac{d_y}{d_c} - \frac{t_c}{d_c} \right)^2} \right)}$$

d_c / λ_g decreases monotonically as both d_c / d_x & d_c / d_y increase

Also d_c / λ_g increase monotonically as φ_0 increases

Because $U_s^b / (U_s^b + U_h^b)$ is monotonic function of d_c / λ_g ,
 we expect that robustness to external forces is also a
 monotonic function of d_c / λ_g i.e

$$F_{\text{holding}} \sim \frac{d_c}{\lambda_g}$$

Figure 6: Elastic Hinge Numerical Analysis

5.2 Elastic Hinge

Different from the skew shell, which bends about the principal direction along y-axis, the elastic hinge bends about x-axis.

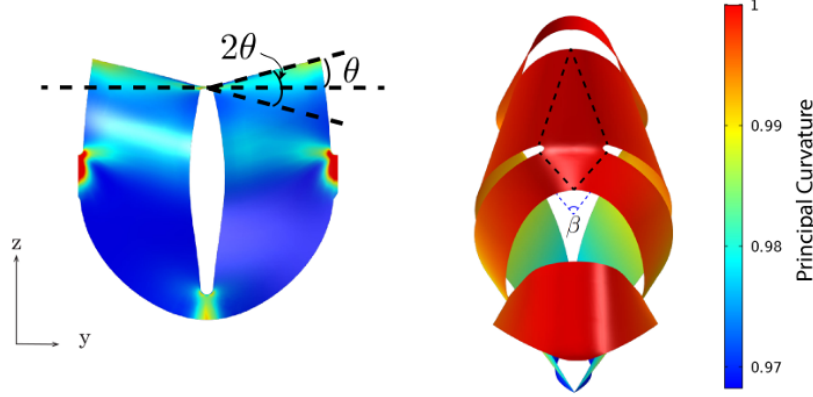


Figure 7: Elastic Hinge

Since t_c is relatively smaller than l_c and l_y , here, we ignore the impact of t_c and use a constant value of 0.8 mm. Fig.S8C shows the energy landscape of the skew shell has a local maximum. This maximum value decays rapidly as we increase c_x and c_y , whereas bending energy of the elastic hinge monotonically decreases as we increase both l_c/l_x and l_c/l_y . Here, we noticed that θ and δ may have an implicit relationship connected by lateral torsional buckling. However, to obtain a closed-form solution, we treat them as two independent variables. The numerical relationship between θ and δ is obtained from FEA simulation and plotted in Fig.8D.

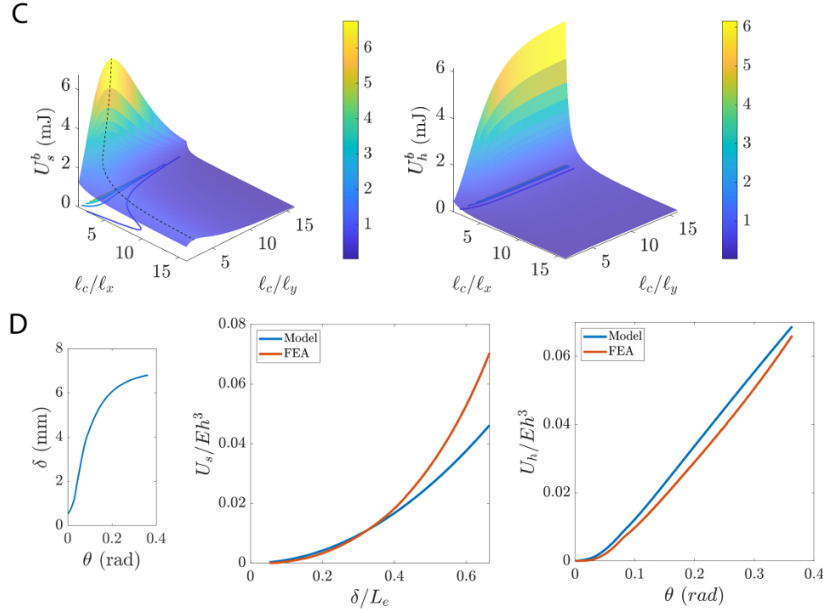


Figure 8: FEM Analysis

Relationship Between Bending Angle (θ) and Deflection (δ):

- At small angles (θ), the deflection increases gradually, indicating linear deformation.
- As θ increases beyond a threshold, δ increases rapidly, showing nonlinear deformation due to lateral torsional buckling.
- This suggests that at high bending angles, the hinge undergoes a structural transition, making it easier to deform further.

Graph: Energy Landscape of the Skew Shell vs. Elastic Hinge:

- The skew shell has a local maximum energy point, meaning there is a peak where energy is stored before deformation occurs.
- The elastic hinge, however, exhibits monotonic energy decrease, meaning its bending energy reduces smoothly as the slit length increases.
- This confirms that the elastic hinge deforms more efficiently and requires less energy for shape morphing than the skew shell.
- As l_c/l_x and l_c/l_y increase, the bending energy decreases, making the hinge more flexible.
- This means that by adjusting these parameters, we can design a gripper with optimized flexibility for different applications.

Finite Element Analysis (FEA) of Deformation:

- Skew Shell Energy (U_s) Increases Non-Linearly – As displacement (δ/L_e) increases, strain energy stored in the skew shell rises non-linearly. The FEA (orange) predicts slightly higher energy than the model (blue) at larger displacements.
- Hinge Energy (U_h) Grows Almost Linearly – The elastic hinge strain energy increases nearly linearly with bending angle (θ), meaning it follows a predictable deformation pattern. The model slightly overestimates energy compared to FEA at higher angles.
- Model vs. FEA Comparison – Both graphs show a close match between theoretical predictions and FEA, with minor deviations at large deformations. The shell model slightly underestimates energy, while the hinge model slightly overestimates it.

6 Conclusion

The Kirigami Soft Gripper leverages patterned cuts and shape morphing to achieve adaptable and efficient grasping. Through theoretical modeling, FEA simulations, and experiments, it demonstrates high success rates in securely holding objects of various shapes and sizes. The gripper's lightweight, flexible design and passive adaptability make it suitable for applications in biomedical handling, industrial automation, and assistive robotics. Future work could enhance materials, actuation mechanisms, and multi-gripper coordination for broader use. This study highlights kirigami's potential in advancing soft robotic systems with simple yet effective grasping solutions.



Figure 9: 3D Printed Kirigami Soft Gripper using TPU

References

- 1 [Shttps://faculty.engineering.asu.edu/acs/wp-content/uploads/sites/33/2021/03/Doroudchi_RoboS_Tracking_for_Soft_Continuum_Robotic_Arms_Using_Inverse_Dynamic_Control_of_a_Cosserat_Rod_Model.pdf](https://faculty.engineering.asu.edu/acs/wp-content/uploads/sites/33/2021/03/Doroudchi_RoboS_Tracking_for_Soft_Continuum_Robotic_Arms_Using_Inverse_Dynamic_Control_of_a_Cosserat_Rod_Model.pdf)
- 2 <https://www.science.org/doi/10.1126/scirobotics.abd6426>
- 3 <https://ieeexplore.ieee.org/document/10635088>
- 4 https://www.researchgate.net/publication/353197467_Analysis_of_soft_kirigami_unit_cells_for_tunable_grasping